Signal Processing 231 (2025) 109897

Contents lists available at ScienceDirect

Signal Processing

journal homepage: www.elsevier.com/locate/sigpro

Pruned DCT precoding-based FBMC modulation: An SC-FDMA inspired approach

Ying Wang [a], Qiang Guo [a], Jianhong Xiang [a,b,*], Yu Zhong [b]

[a] College of Information and Communication Engineering, Harbin Engineering University, Harbin 150001, China
[b] Agile and Intelligent Computing Key Laboratory, China Electronic Technology Group (CETC-10), Chengdu 610036, China

ARTICLE INFO

Dataset link: https://github.com/WangYeeng/Pruned-DCT-P-FBMC_master

Keywords:
OQAM-FBMC
Pruned DCT-p-FBMC
SC-FDMA
Channel coding

ABSTRACT

Filter Bank Multi-Carrier modulation based on Offset Quadrature Amplitude Modulation (FBMC-OQAM) provides superior spectral properties than Orthogonal Frequency Division Multiplexing (OFDM). However, the compatibility of FBMC-OQAM with OFDM in many techniques faces great challenges. In this paper, we present a Pruned Discrete Cosine Transform (DCT) Precoding based FBMC (Pruned DCT-p-FBMC) modulation, which inherits the advantages of FBMC-OQAM as well as Single Carrier Frequency Division Multiple Access and realizes the technical compatibility between FBMC and OFDM. Specifically, considering the anti-interference ability of symbols, we first use pruned DCT to spread them into frequency domain, thus reducing the interference between adjacent symbols. Secondly, we calculate the signal-to-interference ratio and the signal-to-interference-to-noise ratio to assess the impact of residual interference on the system. Finally, the Log-Likelihood Ratio is calculated so that Turbo coding in Pruned DCT-p-FBMC is implemented. Additionally, we provide throughput calculations for evaluating the performance of channel coding and link adaptation. Simulation results show that Pruned DCT-p-FBMC exhibits robust MIMO transmission capabilities along with considerable throughput.

1. Introduction

Future new waveforms for wireless systems should fulfill the requirements of high spectral efficiency, high scalability, and flexible compatibility with other techniques. Specifically, the 5G New Radio (NR) should support diverse use cases, including Band-Delay Transmission and Machine-Type Communication [1], etc. Filter Bank Multi-Carrier modulation based on Offset Quadrature Amplitude Modulation (FBMC-OQAM) is considered as an important candidate for future NR. The reason is that the Out-of-Band (OOB) emission of FBMC-OQAM is significantly lower than that of Orthogonal Frequency Division Multiplexing (OFDM) [2–4]. FBMC-OQAM (simplified as FBMC) is suitable for asynchronous transmission and enables flexible allocation of time–frequency resource for different application situations [5–7]. Although the 3rd Generation Partnership Project (3GPP) failed to select FBMC as the new waveform for 5G, the technology is still the key research topic for future wireless systems [8].

However, restricted by the Balian-Low theorem [9], the orthogonality of FBMC holds only in the real domain. This leads to systems with inherent imaginary interference and significant challenges in channel estimation and Multiple Input Multiple Output (MIMO) implementation [10–12]. On the other hand, the superior spectral properties of FBMC are restricted by the limited resolution in Digital-to-Analog Converter, and by the fact that the power amplifier is nonlinear [6,10]. Therefore, the implementation of FBMC requires strict linearity conditions. M. Payaró et al. [13] and P. Chevalier et al. [14] both realized the combination of MIMO and FBMC. However, they have significant shortcomings. For example, [13] relies heavily on channel information and [14] features high complexity. H. Wang et al. [15] achieved MIMO-FBMC channel estimation by exploiting the sparsity of the channel. Although the complexity of the channel estimation scheme is reduced, the Bit Error Rate (BER) performance of the system is undesirable, and the underlying logic for the combination of MIMO and FBMC is not provided. R. Zakaria et al. [16] used Fast Fourier Transform (FFT) to spread the symbols into the time (or frequency) domain, thus eliminating imaginary interference and realizing the combination of MIMO and FBMC. However, the utilization of FFT not only elevates system complexity but also leads to residual interference. R. Zakaria et al. noted in [12] that symbol spreading can also be achieved using the Discrete Fourier Transform (DFT). However, R. Nissel et al. [17,18] argue that the Hadamard matrix-based spreading scheme is superior to the DFT spreading scheme. They assert that the biorthogonality of the FBMC is perfectly restored within the spread block, with lower

* Corresponding author at: College of Information and Communication Engineering, Harbin Engineering University, Harbin 150001, China.
E-mail addresses: wangyingstu@163.com (Y. Wang), guoqiang@hrbeu.edu.cn (Q. Guo), xiangjianhong@hrbeu.edu.cn (J. Xiang), jade.zhong@hotmail.com (Y. Zhong).

https://doi.org/10.1016/j.sigpro.2025.109897
Received 7 April 2024; Received in revised form 4 January 2025; Accepted 12 January 2025
Available online 20 January 2025

complexity. For the purpose of reducing the FBMC Peak-to-Average Power Ratio (PAPR), R. Nissel et al. [19] proposed a Pruned DFT spread scheme. The scheme not only reduces the PAPR, but also restores the biorthogonality of FBMC and improves the spectral efficiency. Moreover, Pruned DFT-Spread FBMC is similar to Single Carrier Frequency Division Multiple Access (SC-FDMA) adopted by Long Term Evolution (LTE) in the uplink (Note that DFT-OFDM is essentially the same as SC-FDMA.) [20]. However, Pruned DFT-Spread FBMC has residual interference. To mitigate the interference, the author uses a truncated prototype filter, which destroys the real orthogonality of the FBMC, to directly boost the Signal-to-Interference Ratio (SIR), and then, with additional frequency CP. On the other hand, the complex-valued operations required for DFT spread further increase the complexity of the system. The above schemes share a common feature, i.e., restoring the biorthogonality of FBMC, which makes it easy to combine MIMO with FBMC, similar to combining MIMO with OFDM. M. Renfors et al. [21] realized the block Alamouti scheme (symbols are spread into the time domain). The same scheme is utilized in [22], only with the symbols spread into the frequency domain. Both approaches essentially restore the biorthogonality of FBMC through symbol spreading.

Based on the idea of DFT precoding in SC-FDMA, we consider a precoding scheme based on the pruned Discrete Cosine Transform (DCT). This scheme can approximately restore the bi-orthogonality of FBMC and requires only real-valued operations without causing an excessive complexity increase. A similar precoding scheme is employed in [4]. However, the scheme in [4] is highly sensitive to doubly dispersive channels and requires the addition of the guard time slots, which leads to a lower utilization of the time–frequency resources. On the other hand, the Walsh transform-based precoding scheme provides minimal assistance in Peak-to-Average Power Ratio (PAPR) reduction. It is worth noting that, restricted by the Balian-Low theorem, the Pruned DCT-Precoding FBMC still suffers from residual interference. Therefore, our scheme can achieve nearly the same performance as OFDM, particularly in scenarios where interference is not the dominant factor. However, the power of the residual interference is less than −20 dB and has a minimal impact on system reliability. Thus, the residual interference can be ignored, or we can adopt the space–time block coding technique to address the impact of residual interference on reliability. Our main contributions are summarized below:

1. The Pruned DCT precoding based FBMC modulation scheme is presented. Considering the anti-interference capability of QAM symbols, we adopt pruned DCT to spread them into the frequency domain, thus reducing the interference between adjacent symbols. This helps to improve the robustness of the system to multipath and reduces the synchronization requirements. For the base pulse, the pruned DCT matrix reshapes it to approximately restore the FBMC orthogonality. This helps to improve the compatibility of the system with OFDM and enhance the efficiency of spatial multiplexing. See Section 3.
2. We analyze the Signal Interference Ratio (SIR) as well as the Signal-to-Interference-Noise Ratio (SINR) of the Pruned DCT-p-FBMC. Although we restore the bi-orthogonality of the FBMC, numerically the Pruned DCT-p-FBMC still has a few residual interferences, and the channel also induces interference. Through the analysis of the SIR, we can directly evaluate the performance of the system. Moreover, the influence of noise cannot be disregarded; therefore, we utilize the SINR as a pivotal evaluation metric. See Section 4.1.
3. We offer Log Likelihood Ratio (LLR) calculations, facilitating Turbo coding within the Pruned DCT-p-FBMC. Concurrently, we provide throughput calculations to assess the efficacy of channel coding and link adaptation. See Section 4.2.

Notation: Bold uppercase and lowercase letters denote matrix and vector, respectively. $\mathrm{diag}\{\cdot\}$ denotes the diagonal elements of a matrix or generates a diagonal matrix. $\mathrm{Tr}\{\cdot\}$ denotes the trace of a matrix. $\mathbb{E}\{\cdot\}$ denotes the expectation. $\Re\{\cdot\}$ and $\Im\{\cdot\}$ denote the extraction for real and imaginary part operations, respectively. $\otimes$ and $\circ$ denote the Kronecker and Hadamard products, respectively. $(\cdot)^*$, $(\cdot)^{-1}$, $(\cdot)^T$ and $(\cdot)^H$ denote conjugate, inverse, transpose, and conjugate transpose operations respectively. Imaginary unit is denoted as $\mathrm{j} = \sqrt{-1}$. $\mathbf{I}_n$ denotes the $n \times n$ unit matrix. The real domain is denoted by $\mathbb{R}$. The complex domain is denoted by $\mathbb{C}$.

2. FBMC-OQAM model

In FBMC, the transmitted signal is composed of a set of real-valued OQAM symbols. Due to the OQAM symbol spacing being smaller than its duration, we transmit two interleaved OQAM symbols instead of one QAM symbol, thus guaranteeing the transmitted amount of data. Let us assume that the multiplexed FBMC signal $s(t)$ consists of L subcarriers and K time symbols, which can be expressed as

$$s(t) = \sum_{l=1}^{L}\sum_{k=1}^{K} x_{l,k} \underbrace{p_{TX}(t-kT)\mathrm{e}^{\mathrm{j}2\pi lF(t-kT)}\mathrm{e}^{\mathrm{j}\frac{\pi}{2}(l+k)}}_{g_{l,k}(t)}, \tag{1}$$

where $x_{l,k}$ denotes the real-valued OQAM symbol at the time–frequency position (l,k). F denotes the frequency spacing and T the time spacing. $\mathrm{e}^{\mathrm{j}\pi(l+k)/2}$ represents the phase shift factor between adjacent subcarriers and symbols. $g_{l,k}(t)$ denotes the base pulse, which is obtained by combining the time–frequency shifted prototype filter $p(t)$ with the phase shift factor. Note that we assume the prototype filter $p(t)$ is zero outside the time interval $-OT \le t \le OT$. In FBMC, the symbol density $TF = 0.5$ for OQAM corresponds to the symbol density $TF = 1$ for QAM [19]. The received signal $r(t)$ can be described by convolving $s(t)$ with the time-varying multipath channel $h(t,\tau)$ [23], denoted by

$$\begin{aligned} & r(t) = \int_{\mathbb{R}} h(t,\tau)\, s(t-\tau)\,\mathrm{d}\tau + \bar{\mathrm{n}}(t) \\ & st.\ h(t,\tau) = \frac{1}{\sqrt{P}} \sum_{p=1}^{P} \eta_p(t)\, \mathrm{e}^{\mathrm{j}2\pi t(f_{DP}+\varphi_P)} \delta_{\tau-\tau_p} \end{aligned}, \tag{2}$$

where P denotes the number of paths, and $\eta_p(t)$ the attenuation factor of the pth path. f_{Dp} and φ_p denote the Doppler shift and initial phase, respectively. δ_t denotes the Dirac delta function. τ_p denotes the time delay of the pth path. $\bar{\mathrm{n}}(t)$ denotes white noise. At the receiver, by performing inverse mapping of the received signal to the base pulse, we can obtain the received symbol $y_{l,k}$ at the time–frequency position (l,k), denoted as

$$y_{l,k} = \int_{\mathbb{R}} r(t)\, g^*_{l,k}(t)\,\mathrm{d}t. \tag{3}$$

Due to FBMC compressing the time–frequency spacing to half of the original one, the orthogonality of the system holds only in the real domain [6], expressed as

$$\begin{aligned} & \Re\left\{\left\langle g_{l,k}(t), g_{l',k'}(t)\right\rangle\right\} \\ & = \Re\left\{\int_{\mathbb{R}} g_{l,k}(t) g^*_{l',k'}(t)\mathrm{d}t\right\} = \delta_{\mathcal{D}_l,\mathcal{D}_k}, \end{aligned} \tag{4}$$

where $\mathcal{D}_l = l - l'$ and $\mathcal{D}_k = k - k'$. $\delta_{i,j}$ denotes the Kronecker delta function. The orthogonality condition of Eq. (4) leads to imaginary interference. For precise analysis, we define the interference term as

$$\zeta_{l,k}^{l',k'} = \int_{\mathbb{R}} g_{l,k}(t) g^*_{l',k'}(t)\mathrm{d}t, \tag{5}$$

where if $(l,k) = (l',k')$, then $\zeta_{l,k}^{l',k'} = 1$; If $(l,k) \neq (l',k')$, then $\zeta_{l,k}^{l',k'}$ is purely imaginary. Combining Eqs. (1) and (5), we can rewrite Eq. (3)

as

$$\begin{aligned} y_{l,k} &= \int_{\mathbb{R}} \left(\int_{\mathbb{R}} h(t,\tau) \sum_{l}\sum_{k} x_{l,k} g_{l,k}(t-\tau)\,\mathrm{d}\tau + \bar{\mathrm{n}}(t) \right) g_{l,k}^{*}(t)\,\mathrm{d}t \\ &= \sum_{l}\sum_{k} x_{l,k} \iint_{\mathbb{R}} h(t,\tau) g_{l,k}(t-\tau) g_{l,k}^{*}(t)\,\mathrm{d}\tau \mathrm{d}t \\ &\quad + \int_{\mathbb{R}} \bar{\mathrm{n}}(t) g_{l,k}^{*}(t)\,\mathrm{d}t \\ &= H_{l,k} x_{l,k} + \sum_{l\neq l'}\sum_{k\neq k'} H_{l',k'} x_{l',k'} \zeta_{l,k}^{l',k'} + \mathrm{n}_{l,k} \end{aligned}, \tag{6}$$

where $H_{l,k} = \iint_{\mathbb{R}} h(t,\tau) g_{l,k}(t-\tau) g_{l,k}^{*}(t)\,\mathrm{d}\tau\mathrm{d}t$ is the one-tap channel at time–frequency position (l,k), which is approximately equal to the time-varying transfer function [19]. Thereby, $H_{l,k}$ also can be obtained by discretizing the transfer function $H(t,f)$, denoted as

$$H_{l,k} = H(kT, lF). \tag{7}$$

$\mathrm{n}_{l,k}$ denotes the noise term at the time–frequency position (l,k), expressed as

$$\mathrm{n}_{l,k} = \int_{\mathbb{R}} \bar{\mathrm{n}}(t) g_{l,k}^{*}(t)\mathrm{d}t. \tag{8}$$

The described continuous-time system provides a physical insight into FBMC. The generation of FBMC signals can rely on Polyphase Networks (PPN) [24,25]. However, in practice, the signals are time discrete. Therefore, we discretize time and adopt matrix theory to describe FBMC. Considering the Inverse Fast Fourier Transform and Fast Fourier Transform (IFFT/FFT) implementation schemes of the FBMC [26], we sample the base pulse in Eq. (1) with the rate $f_s = FN_{FFT}$. If the sampled values are represented by a vector $\mathbf{g}_{l,k} \in \mathbb{C}^{N\times 1}$, then the elements of $\mathbf{g}_{l,k} \in \mathbb{C}^{N\times 1}$ can be expressed as

$$\left[\mathbf{g}_{l,k}\right]_n = \frac{1}{\sqrt{FN_{FFT}}} g_{l,k}\left(\frac{n-1}{FN_{FFT}} - (O-1)T \right), \tag{9}$$

where $n = 1,\dots,N$, with N denoting the total sample number. O denotes the overlapping factor, and N_{FFT} the FFT size. Note that in FBMC, the base pulse will span O symbol periods. Therefore, the time range for the specific symbol is $\left(-\frac{(O-1)T}{2}, \frac{(O-1)T}{2}\right)$. To ensure correct sampling, the center of the base pulse needs to be shifted by $(O-1)T$ to align with the reference time point. Then, according to Eq. (9), we integrate all the base pulse vectors into the transmission matrix $\mathbf{G} = \left[\mathbf{g}_{1,1},\dots,\mathbf{g}_{L,K}\right] \in \mathbb{C}^{N\times LK}$. For a wireless channel, we adopt a banded convolution matrix $\mathbf{H} \in \mathbb{C}^{N\times N}$ for modeling [6,11,27]. The matrix model for the whole transmission system can be expressed as

$$\mathbf{y} = \mathbf{G}^H\mathbf{H}\mathbf{G}\mathbf{x} + \mathbf{n}, \tag{10}$$

where $\mathbf{x} = \left[x_{1,1},\dots,x_{L,K}\right]^T \in \mathbb{C}^{LK\times 1}$ denotes the transmitted symbol and $\mathbf{y} = \left[y_{1,1},\dots,y_{L,K}\right]^T \in \mathbb{C}^{LK\times 1}$ the received symbol. $\mathbf{n} \sim \mathcal{CN}(\mathbf{0}, P_{\mathrm{n}}\mathbf{G}^H)$ denotes the complex Gaussian noise matrix. If the Doppler spread of the channel is low, the interference induced by the channel can be neglected [6]. Thus, we can rewrite Eq. (10) as

$$\mathbf{y} \approx \mathrm{diag}\left\{\mathbf{G}^H\mathbf{H}\mathbf{G}\right\}\mathbf{G}^H\mathbf{G}\mathbf{x} + \mathbf{n}. \tag{11}$$

Note that Eq. (11) is a simplified version for low-Doppler spread cases with higher computational efficiency, while Eq. (10) is suitable for a wider range of channel conditions. Thus, in channels with high Doppler spread, we still use Eq. (10). To make Eqs. (10)–(11) easier to understand, we provide a detailed derivation in Appendix A. The imaginary interference in FBMC is characterized by the off-diagonal elements of $\mathbf{G}^H\mathbf{G}$, while the condition for real orthogonality is represented by $\Re\left\{\mathbf{G}^H\mathbf{G}\right\} = \mathbf{I}_{LK}$. Without loss of generality, we provide an explanation of the IFFT/FFT realization process for FBMC using the sampled signals of Eq. (1). The sampled signal of Eq. (1) can be expressed as

$$s(\tilde{n}\Delta t) = p(\tilde{n}\Delta t)\sum_{k=1}^{K}\sum_{l=1}^{L} \mathrm{e}^{\mathrm{j}2\pi l(\tilde{n}/N_{FFT}-k/2\ )} x_{l,k}\mathrm{e}^{\mathrm{j}\pi(l+k)/2}, \tag{12}$$

where $\tilde{n} = -ON_{FFT}/2,\dots,ON_{FFT}/2-1$ and $\Delta t = 1/FN_{FFT}$. Note that $p(\tilde{n}\Delta t)$ is an irrelevant term for l and k, which can be placed outside the dual summation. The summation term in Eq. (12) for the subcarriers corresponds to the N_{FFT}-point IFFT, with its transformed object is $\vec{\mathbf{x}}_k = \left[0, x_{1,k}\mathrm{e}^{\mathrm{j}\pi(1+k)/2},\dots,x_{L,k}\mathrm{e}^{\mathrm{j}\pi(L+k)/2},0,\dots\right]^T \in \mathbb{C}^{N_{FFT}\times 1}$. The symbols of all time positions are then obtained by time shifting. The receiver operates similarly to the transmitter, but in reverse order, involving an N_{FFT}-point FFT.

3. Pruned DCT precoding FBMC

The proposed Pruned DCT precoding based FBMC has two interpretations:

(1) For transmitted symbols, the transmitted complex symbols are pre-coded to replace the complex-to-real conversion in conventional FBMC. Note that we still compress the time–frequency spacing to $TF = \frac{1}{2}$, thus ensuring the spectral efficiency of the system.

(2) For the base pulse, the duration of the base pulse is significantly compressed, thereby enhancing the system's robustness against time-varying channels.

Each of the two interpretations contributes to signal generation and facilitates understanding of orthogonality. The first interpretation offers flexibility and theoretical insights into efficiently generating signals. The second interpretation provides the underlying logic for understanding the restoration of bi-orthogonality in Pruned DCT-p-FBMC. Note that Pruned DCT-p-FBMC can achieve OFDM-like orthogonal transmission.

3.1. Symbol precoding & decoding

In FBMC, the QAM complex symbol that can be transmitted in the $L\times K$ 2-D plane after compression of the time–frequency spacing is $\tilde{x}_{\ell,k}$, where $\ell \in \left[1,\dots,L/2\right]$. For the k complex symbol of length $L/2$, we pre-code it using DCT [28], denoted by

$$x_{l,k} = \sqrt{\frac{2}{L}}\sum_{\ell=1}^{L/2}\tilde{x}_{\ell,k}\frac{1}{\sqrt{1+\delta_{l-1}}}\cos\left(\frac{\pi}{2L}(4\ell-3)(l-1)\right). \tag{13}$$

Note that instead of utilizing the full DCT, we select its odd dimensions with equal intervals. At the receiver, by applying IDCT to the received symbols, we can obtain the decoded received QAM complex symbol $\tilde{y}_{\ell,k}$, denoted by

$$\tilde{y}_{\ell,k} = \sqrt{\frac{2}{L}}\sum_{l=1}^{L} y_{l,k}\frac{1}{\sqrt{1+\delta_{\ell-1}}}\cos\left(\frac{\pi}{2L}(l-1)(4\ell-3)\right). \tag{14}$$

For achieving optimal symbol detection, we recommend implementing equalization techniques prior to decoding. Such operation of precoding data symbols enables direct signal generation. However, the operation is not conducive to understanding orthogonality restoration.

Now, we interpret Eqs. (13)–(14) by matrix form to understand orthogonality intuitively. The precoding matrix $\boldsymbol{\varphi} \in \mathbb{R}^{L\times L/2}$, which only contains the DCT coefficients for one symbol, can be obtained directly by applying the DCT transform to the unit array, that is

$$\boldsymbol{\varphi} = \left[\mathcal{F}_{dct}\left(\mathbf{I}_L\right)\right]_{:,2l-1} = \boldsymbol{\mathcal{D}}_{L\times\frac{L}{2}}, \tag{15}$$

where $\mathcal{F}_{dct}(\cdot)$ denotes the DCT operation. $\boldsymbol{\mathcal{D}}_{L\times\frac{L}{2}}$ denotes the $L\times\frac{L}{2}$ DCT matrix. By mapping the precoding matrix of one symbol to all symbols, we can directly implement the precoding of the transmitted symbol $\tilde{\mathbf{x}} = \left[\tilde{x}_{1,1},\dots,\tilde{x}_{L/2,K}\right]^T \in \mathbb{C}^{LK/2\times 1}$, denoted as

$$\mathbf{x} = \underbrace{\boldsymbol{\varphi}\otimes\mathbf{I}_K}_{\boldsymbol{\phi}}\tilde{\mathbf{x}}, \tag{16}$$

where $\boldsymbol{\phi} \in \mathbb{R}^{LK\times LK/2}$ denotes the precoding matrix for all symbols. At receiver side, we use decoding matrix $\boldsymbol{\phi}^H \in \mathbb{C}^{LK/2\times LK}$ to decode the

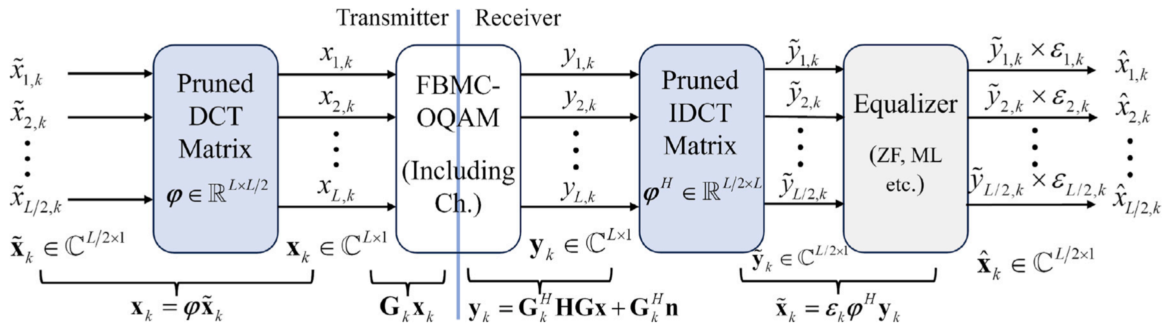

Fig. 1. Pruned DCT-p-FBMC transmission structure at time position k. Different from conventional FBMC, the complex-real conversion of QAM symbols is replaced by a pruned DCT transform. $\varepsilon_{\ell,k}$ denotes the one-tap equalization operator.

received symbols. Thereby, the received complex symbol $\tilde{\mathbf{y}} \in \mathbb{C}^{LK/2\times 1}$ is obtained, denoted as

$$\tilde{\mathbf{y}} = \boldsymbol{\phi}^H \mathbf{y}. \tag{17}$$

Fig. 1 shows the Pruned DCT precoding based FBMC transmission architecture which incorporates equalization techniques. FBMC has inherent interference that makes channel estimation and equalization more challenging. Pruned DCT-p-FBMC can greatly simplify the equalization due to the restoration of bi-orthogonality, see Section 5, and channel estimation will also be simplified. For example, the LTE pilot structure can be used directly. However, we currently investigate only equalizers. The problem of channel estimation is considered to be completed in future work. From Eq. (16), we know that $\boldsymbol{\phi} \in \mathbb{R}^{LK\times LK/2}$ is a sparse block diagonal matrix. When the number of subcarriers is $L = 4$, the specific value of subblock $\boldsymbol{\varphi} \in \mathbb{R}^{L\times L/2}$ within matrix $\boldsymbol{\phi} \in \mathbb{R}^{LK\times LK/2}$ can be expressed as

$$\boldsymbol{\varphi} = \begin{bmatrix} 0.5 & 0.6533 & 0.5 & 0.2706 \\ 0.5 & -0.2706 & -0.5 & 0.6533 \end{bmatrix}^T. \tag{18}$$

The precoding matrix allows the transmitted symbols to retain the complexity property. Note that in conventional FBMC, $\mathbf{x}_k \in \mathbb{R}^{L\times 1}$ is real-valued data symbol.

3.2. Pulse orthogonality approximation

We now discuss the properties of the base pulse. In the matrix form of modeling, if the Pruned DCT matrix is considered to be combined with the base pulse (i.e., $\tilde{\mathbf{G}} = \mathbf{G}\boldsymbol{\phi}$), then the regular base pulse $\mathbf{g}_{l,k}$ can be regarded as the new pulse $\tilde{\mathbf{g}}_{l,k}$, see Fig. 2. $\tilde{\mathbf{g}}_{l,k}$ can also be interpreted as the output waveform of the precoder when the transmitted symbol $\tilde{x}_{\ell,k}$ is 1. On the other hand, our Pruned DCT-p-FBMC can employ the same prototype filters as conventional FBMC, including PHYDYAS [26], Hermite [29], and IOTA [30], etc. Throughout this paper, unless otherwise stated, we consistently employ the PHYDYAS prototype filter. Over an Additive Gaussian White Noise channel (i.e., $\mathbf{H} = \mathbf{I}_N$), the system orthogonality can be expressed as

$$\tilde{\mathbf{G}}^H \tilde{\mathbf{G}} = \boldsymbol{\phi}^H \mathbf{G}^H \mathbf{G} \boldsymbol{\phi} \approx \mathbf{I}_{LK/2}. \tag{19}$$

Note that orthogonality described by Eq. (19) exists with very small residual interference. Generally, such residual interference has no impact on system performance. However, in practice, we need to consider issues such as latency, OOB emission and system computational complexity.

We first analyze the transmission delay of the system. Neglecting channel delay and processing delay, the transmission time of one FBMC symbol is determined by the overlapping factor O and is given by O/F [19]. However, one OFDM symbol carries twice as much information as one FBMC symbol. Thus, to process the second FBMC symbol, an additional delay of $0.5/F$ is required. For a conventional FBMC subframe containing K time symbols, we can calculate the time

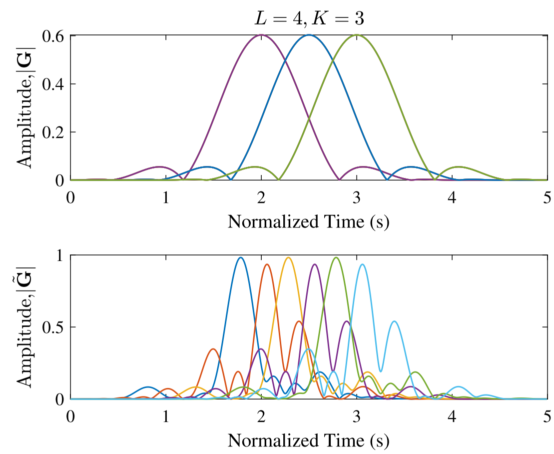

Fig. 2. Amplitude for regular pulses and encoder outputs (i.e., new base pulse) when transmitted symbol is 1. Note that the primary and secondary pulses of the new base pulse together characterize an original pulse. Thus, $\tilde{\mathbf{g}}_{l,k}$ has no specific properties (i.e., without a fixed expression) and is difficult to generate directly.

delay of one frame as

$$T_{\text{frame}} = \frac{O}{F} + \frac{0.5}{F}(K-1). \tag{20}$$

In LTE, the duration of one subframe is 1 ms. The LTE subframe is composed of $K = 14$ OFDM symbols with CP spacing of $T_{CP} = \frac{1}{14F}$ and $F = 15$ kHz. However, the duration for both conventional FBMC and Pruned DCT-p-FBMC subframes is 1.17 ms (i.e., $T_{\text{frame}}\big|_{O=4,F=15\text{ kHz},K=28} \approx 1.17$ ms). Note that to guarantee the same information volume, the number of time symbols should be $K = 28$ and the overlapping factor O is set to 4. Thus, the Pruned DCT-p-FBMC transmission delay is 17% lengthier than LTE.

Secondly, we analyze the OOB emission of the system. We normalize the transmitted power of the FBMC symbols and then calculate the power spectral density $\mathbf{P}_f \in \mathbb{R}^{N\times 1}$ as

$$\mathbf{P}_f = \left| FFT\left(\mathbf{G}_k \boldsymbol{\varphi} \tilde{\mathbf{x}}_k\right)\right|^2, \tag{21}$$

where $FFT\{\cdot\}$ denotes the Fourier transform operation. Note that we similarly normalize the power spectral density and implicitly perform an infinite simulation in time. Fig. 3 shows the power spectral density for different systems. Pruned DCT-p-FBMC has almost the same spectral properties as conventional FBMC and is much better than OFDM as well as SC-FDMA.

Finally, we consider the computational complexity of the system. If the system IFFT/FFT implementation is considered, then the complexity of Pruned DCT-p-FBMC can be expressed as

$$\mathcal{O} = L + 2\left(L\log_2\left(\frac{L}{2}\right) + N_{FFT}\log_2\left(N_{FFT}\right) + ON_{FFT}\right), \tag{22}$$

where $L + 2L\log_2(L/2)$ corresponds to the multiplication numbers for Pruned DCT precoding (the real and imaginary parts with complex

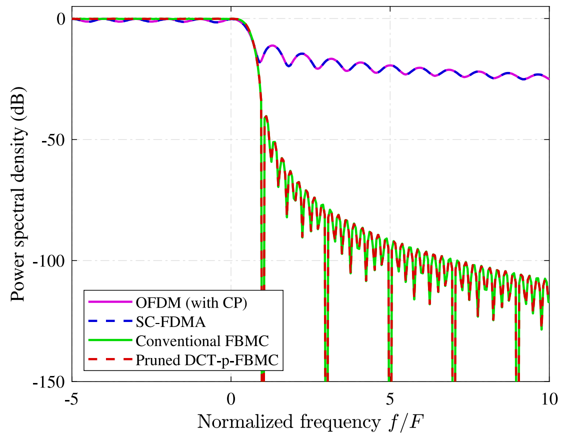

Fig. 3. Pruned DCT-p-FBMC retains the superior spectral properties of conventional FBMC. Although the precoding matrix $\boldsymbol{\varphi}$ reshapes the base pulse, the power and power spectral density of the transmitted signal remain the same as that of the conventional FBMC.

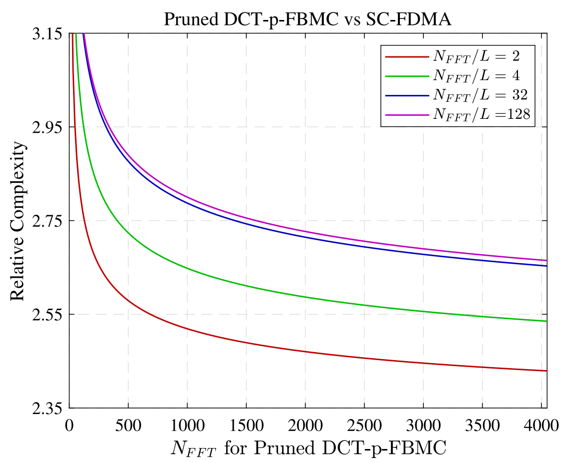

Fig. 4. Relative complexity for Pruned DCT-p-FBMC vs. SC-FDMA with different N_{FFT} and L.

numbers are recorded twice). $N_{FFT}\log_2\left(N_{FFT}\right)$ corresponds to the IFFT required for FBMC. ON_{FFT} corresponds to the multiplication of the prototype filter coefficients required for FBMC. Fig. 4 shows the relative complexity for Pruned DCT-p-FBMC versus SC-FDMA.

The compression of the Pruned DCT-p-FBMC time spacing implies that the complexity must be twice that of SC-FDMA, which is an unavoidable drawback. For example, in LTE, $N_{FFT} = 1024$ and $L = 600$ [19], which leads to a complexity of about 3.9×10^4 for Pruned DCT-p-FBMC and 1.6×10^4 for SC-FDMA. Thus, the complexity of Pruned DCT-p-FBMC is about 2.44 times higher than SC-FDMA. However, the superior performance retained by Pruned DCT-p-FBMC allows it to support a wider range of cases.

4. Residual interference & throughput

We prove that Pruned DCT-p-FBMC approximately restores orthogonality by Eq. (19). However, constrained by the Balian-Low theorem, we find that interference residues exist during numerical computations. Although the order of magnitude for interference residuals is small, we still need to analyze its impact on the system. Particularly in complex channel environments, we need to explore whether Pruned DCT-p-FBMC can maintain the same transmission performance as conventional FBMC.

4.1. SIR & SINR

The inherent imaginary interference of the conventional FBMC is described as the off-diagonal elements of the $\mathbf{G}^H\mathbf{G}$. In Pruned DCT-p-FBMC, we adopt the Pruned DCT matrix to reduce the off-diagonal elements of the $\mathbf{G}^H\mathbf{G}$ to nearly zero. However, some residuals remain in the values, which means that interference between the symbols still exists. We evaluate the interference by SIR. The SIR at time position k can be calculated as

$$\mathrm{SIR}_k = \frac{L/2}{\left\|\tilde{\mathbf{G}}_k^H\tilde{\mathbf{G}}\right\|_F^2 - \mathrm{Tr}\left\{\tilde{\mathbf{G}}_k^H\tilde{\mathbf{G}}\right\}}, \tag{23}$$

where $\|\cdot\|_F$ denotes the Frobenius paradigm and $\tilde{\mathbf{G}}_k^H = \boldsymbol{\varphi}^H\mathbf{G}_k^H$. Eq. (23) is highly related to the number of subcarriers L. Like LTE, SIR can reach more than 40 dB when $L = 600$. Thus, the residual interference can be ignored. However, in practice, SIR should also include channel-induced interference. We introduce the channel convolution matrix $\mathbf{H} \in \mathbb{C}^{N\times N}$ and consider an efficient SIR calculation method. Firstly, we can directly calculate the signal power $P_{S_{\ell,k}\&I_{\ell,k}} = \mathbb{E}\left\{\left|\tilde{y}_{\ell,k}\right|^2\right\}$ including interference, denoted as

$$P_{S_{\ell,k}\&I_{\ell,k}} = \sum_{i=1}^{LK/2}\sum_{n=1}^{N}\left[\left|\tilde{\mathbf{G}}^T\boldsymbol{\mathcal{R}}\circ\tilde{\mathbf{G}}^H\right|\right]_{i,n}, \qquad st.\quad \boldsymbol{\mathcal{R}} = \left(\mathbf{I}_N\otimes\tilde{\boldsymbol{\varphi}}^H\mathbf{G}^H\right)\mathbf{R}_{\mathrm{H}}\left(\mathbf{I}_N\otimes\mathbf{G}\tilde{\boldsymbol{\varphi}}\right) \tag{24}$$

where $\mathbf{R}_{\mathrm{H}} = \mathbb{E}\left\{\mathrm{vec}\left\{\mathbf{H}\right\}\mathrm{vec}\{\mathbf{H}\}^H\right\}$ denotes the channel correlation matrix. $\tilde{\boldsymbol{\varphi}} \in \mathbb{R}^{LK\times 1}$ denotes the $\ell + \frac{L(k-1)}{2}$th column of the matrix $\boldsymbol{\phi} \in \mathbb{R}^{LK\times LK/2}$. Secondly, we calculate the signal power $P_{S_{\ell,k}}$, denoted as

$$P_{S_{\ell,k}} = \max_{1\le i\le LK/2}\sum_{n=1}^{N}\left[\left|\tilde{\mathbf{G}}^T\boldsymbol{\mathcal{R}}\circ\tilde{\mathbf{G}}^H\right|\right]_{i,n}. \tag{25}$$

Finally, according to Eqs. (24)–(25), we can calculate the SIR at time position k, denoted as

$$\mathrm{SIR}_k = \frac{\sum_{\ell=1}^{L/2} P_{S_{\ell,k}}}{\sum_{\ell=1}^{L/2}\left(P_{S_{\ell,k}\&I_{\ell,k}} - P_{S_{\ell,k}}\right)}. \tag{26}$$

Now, we consider time-varying channels with different tap delays. Fig. 5 shows the curves of SIR versus velocity for different delay spreads. Pruned DCT-p-FBMC is more robust to time-varying channels than CP-OFDM ($T_{CP} = 4.76$ µs) and SC-FDMA. This conclusion can be drawn in two aspects:

(1) In theoretical terms, with DCT precoding, the data symbols are spread in frequency domain, resulting in the Doppler effect being dispersed. Moreover, symbols at different frequencies are no longer strongly correlated, resulting in the fading effect being smoothed.
(2) In numerical terms, Pruned DCT-p-FBMC shows a better SIR than CP-OFDM in time-varying channels, see Fig. 5.

So far, we have ignored noise, but now take it into our consideration. The input–output relationship of the whole transmission system (see Fig. 1, including equalization) can be expressed as

$$\hat{\mathbf{x}} = \mathrm{diag}\left(\boldsymbol{\varepsilon}\right)\boldsymbol{\phi}^H\mathbf{G}^H\mathbf{H}\tilde{\mathbf{G}}\tilde{\mathbf{x}} + \mathrm{diag}\left(\boldsymbol{\varepsilon}\right)\boldsymbol{\phi}^H\mathbf{n}, \tag{27}$$

where $\mathrm{diag}\left(\boldsymbol{\varepsilon}\right) \in \mathbb{C}^{LK/2\times LK/2}$ with $\boldsymbol{\varepsilon} \in \mathbb{C}^{LK/2\times 1}$ denotes the equalization vector and $[\boldsymbol{\varepsilon}]_{\ell+\frac{L(k-1)}{2}} = \varepsilon_{\ell,k}$. Over a doubly flat channel or zero noise environment, the equalization operator can be the Zero Forced (ZF) equalizer $\varepsilon_{\ell,k}^{\mathrm{ZF}} = 1/H_{\ell,k}$. The Minimum Mean Square Error (MMSE) equalizer becomes practical when we consider noise, i.e., $\varepsilon_{\ell,k}^{\mathrm{MMSE}} = H_{\ell,k}^*/(|H_{\ell,k}|^2 + P_{\mathrm{n}})$. Over time-varying channels, we need to introduce a scaling factor to ensure that the data symbols are estimated approximately unbiased (i.e., $\mathbb{E}\left\{\hat{x}_{\ell,k}\left|\tilde{x}_{\ell,k}\right.\right\} \approx \tilde{x}_{\ell,k}$). This indicates that unbiased estimation needs to ensure that the expectation of $\hat{x}_{\ell,k}$ is approximately equal to $\tilde{x}_{\ell,k}$, and thus that the bit-inverse mapping is

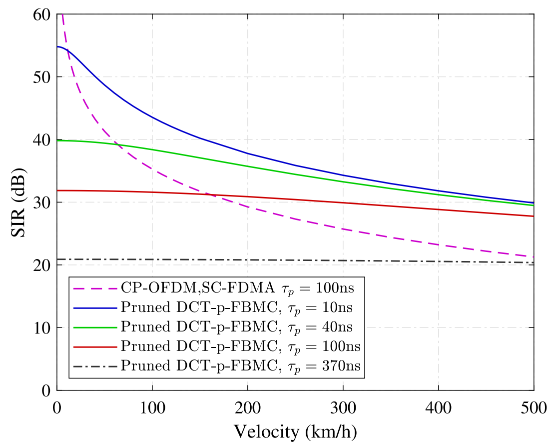

Fig. 5. Extra interference induced by time-varying channels. Pruned DCT-p-FBMC is more robust to time-varying channels. Note that the SIR of CP-OFDM is not impacted by the channel delay spread because the CP time spacing $T_{CP} \geq \tau_{\max}$.

correct. Thus, the MMSE equalization operator can be expressed as

$$\begin{aligned}\varepsilon_{\ell,k} &= \frac{\varepsilon_{\ell,k}^{MMSE}}{\frac{1}{L}\sum_{l=1}^{L}\frac{1}{1+P_{\mathrm{n}}/|H_{\ell,k}|^2}} \\ &= \frac{LH_{\ell,k}^*}{\left(\left|H_{\ell,k}\right|^2+P_{\mathrm{n}}\right)\sum_{l=1}^{L}\frac{1}{1+P_{\mathrm{n}}/|H_{\ell,k}|^2}}.\end{aligned} \tag{28}$$

For uncorrelated data symbols with unit power and uncorrelated noise with power P_{n}, SINR can be calculated according to Eq. (27) as

$$\begin{aligned}&\mathrm{SINR}_{\ell,k}(\mathbf{H}) \\ &= \frac{1}{\sum_{i=1}^{LK/2}\left|[\bar{\boldsymbol{\Lambda}}]_{\tilde{l},i}\right|^2 + P_{\mathrm{n}}\sum_{n=1}^{N}\left|\left[\mathrm{diag}(\boldsymbol{\varepsilon})\,\boldsymbol{\phi}^H\mathbf{G}^H\right]_{\tilde{l},n}\right|^2},\end{aligned} \tag{29}$$

where $\bar{\boldsymbol{\Lambda}} = \mathrm{diag}(\boldsymbol{\varepsilon})\,\boldsymbol{\phi}^H\mathbf{G}^H\mathbf{H}\tilde{\mathbf{G}} - \mathbf{I}_{LK/2}$ and $\tilde{l} = \ell + L(k-1)/2$. Note that the SINR of Pruned DCT-p-FBMC is slightly lower than that of the other systems due to the orthogonality error. Eq. (29) incorporates the channel-induced interference as well as the orthogonality error. Thus, $\mathrm{SINR}_{\ell,k}(\mathbf{H})$ will be an important parameter for calculating the throughput of the system.

4.2. Throughput

The Pruned DCT-p-FBMC approximately restores the bi-orthogonality, which means that it can be approximately equivalent to the conventional OFDM model (without equalization techniques), expressed as

$$\begin{aligned}\tilde{\mathbf{y}} &= \tilde{\mathbf{G}}^H\mathbf{H}\tilde{\mathbf{G}}\tilde{\mathbf{x}} + \tilde{\mathbf{n}} \\ &\approx \tilde{\mathbf{h}}\tilde{\mathbf{G}}^H\tilde{\mathbf{G}}\tilde{\mathbf{x}} + \tilde{\mathbf{n}}, \\ &= \tilde{\mathbf{h}}\tilde{\mathbf{x}} + \tilde{\mathbf{n}}\end{aligned} \tag{30}$$

where $\tilde{\mathbf{h}} = \mathrm{diag}\left\{\tilde{\mathbf{G}}\mathbf{H}\tilde{\mathbf{G}}\right\} \in \mathbb{C}^{LK/2\times LK/2}$, $\tilde{\mathbf{G}}^H\tilde{\mathbf{G}} \approx \mathbf{I}_{LK/2}$ and $\tilde{\mathbf{n}} \sim \mathcal{CN}\left(0, P_{\mathrm{n}}\tilde{\mathbf{G}}^H\right)$. Note that whether the approximation of Eq. (30) holds or not depends on many factors, including transmission time, channel coherence time, residual interference level, and noise level, etc. Thus, it is not very accurate to consider the approximation of Eq. (30) to be held simply by the transmission time being less than the channel coherence time. If the noise level in the transmission medium is higher than the residual interference, then the approximation of Eq. (30) holds. At this point, the approximation error depends on the noise. If the noise level in the transmission medium is lower than the residual interference, then the approximation of Eq. (30) does not hold. At this point, the system requires a more complex equalizer. In many practical cases, the SNR is below 20 dB [17]. Thus, based on the conclusions of Fig. 5, we always consider that the approximation of Eq. (30) holds. Once the approximation of Eq. (30) holds, FBMC is compatible with OFDM. Thereby, many techniques of OFDM can be directly adopted for FBMC, such as: turbo coding, ML detection and Alamouti's space–time block code. Particularly, FBMC can be directly combined with MIMO technology without additional operations.

For a fair comparison of the different multicarrier modulations' performance, we employ throughput as a metric. Because throughput incorporates channel coding and link adaptation. For channel coding, we consider the Turbo coding scheme based on the LTE standard. The LLR required for Turbo decoding is calculated with AWGN channels for each symbol. Thus, the main feature for LLR is the SINR of Eq. (29). Over an AWGN channel, we can maximally simplify the LLR calculation, denoted as

$$LLR\left(b_i\right) = \log\frac{\sum_{\tilde{x}_{\ell,k}\in\chi_1^i}\exp\left\{-\left|\frac{\tilde{y}_{\ell,k}-\tilde{x}_{\ell,k}}{P_{\mathrm{n}}}\right|^2\right\}}{\sum_{\tilde{x}_{\ell,k}\in\chi_0^i}\exp\left\{-\left|\frac{\tilde{y}_{\ell,k}-\tilde{x}_{\ell,k}}{P_{\mathrm{n}}}\right|^2\right\}}, \tag{31}$$

where b_i denotes the ith bit. χ_1^i and χ_0^i denote the subsets of symbols whose ith bit is 1 and 0, respectively. $P_{\mathrm{n}}^{\ell,k}$ denotes the noise power for the corresponding symbol. If we consider the channel gain, then the LLR can be calculated as

$$\begin{aligned}&LLR\left(b_i\right) \\ &= \log\frac{\sum_{\tilde{x}_{\ell,k}\in\chi_1^i}\frac{1}{\pi P_{\mathrm{n}}^{\ell,k}}\exp\left\{-\left|\mathcal{G}_{\mathrm{n}}^{\ell,k}\left(\tilde{y}_{\ell,k}-\tilde{h}_{\ell,k}\tilde{x}_{\ell,k}\right)\right|^2\right\}}{\sum_{\tilde{x}_{\ell,k}\in\chi_0^i}\frac{1}{\pi P_{\mathrm{n}}^{\ell,k}}\exp\left\{-\left|\mathcal{G}_{\mathrm{n}}^{\ell,k}\left(\tilde{y}_{\ell,k}-\tilde{h}_{\ell,k}\tilde{x}_{\ell,k}\right)\right|^2\right\}},\end{aligned} \tag{32}$$

where $\tilde{h}_{\ell,k} = [\tilde{\mathbf{h}}]_{\ell+L(k-1)/2}$ denotes the one-tap channel corresponding to the data symbol. $P_{\mathrm{n}}^{\ell,k}$ denotes the noise power corresponding to the symbol, and $\mathcal{G}_{\mathrm{n}}^{\ell,k}$ can be calculated as

$$\begin{aligned}&\mathcal{G}_{\mathrm{n}}^{\ell,k} = \sqrt{\left(P_{\mathrm{n}}^{\ell,k}\right)^{-1}} = \mathrm{diag}\left(\mathbf{S}\sqrt{\mathbf{V}}\mathbf{U}^H\right)_{\ell'}, \\ &st.\ \mathbf{R}_{\mathrm{n}}^{-1} = \mathbf{S}\mathbf{V}\mathbf{U}^H\end{aligned} \tag{33}$$

where $\ell' = \ell + L(k-1)/2$, $\mathbf{R}_{\mathrm{n}} \in \mathbb{C}^{LK/2\times LK/2}$ denotes the noise correlation matrix. The detailed derivation of Eq. (33) is provided in Appendix B. Note that $\tilde{\mathbf{G}}^H\tilde{\mathbf{G}} \approx I_{LK/2}$ leads to differences in noise power corresponding to different symbols. Therefore, $\frac{1}{\pi P_{\mathrm{n}}^{\ell,k}}$ cannot be ignored. Eq. (32) can be applied to the direct calculation of LLR in MIMO. However, the singular value decomposition of Eq. (33) leads to additional calculation complexity. Therefore, our alternative is to calculate the LLR using Eq. (31). Adopting the calculated LLR, we can implement Turbo decoding, which enables the complete channel coding process. For throughput, the well-known AWGN channel capacity $C_{\mathrm{AWGN}} = \mathbb{E}\left\{\log_2(1+\mathrm{SNR})\right\}$ is no longer reasonable. The reason is that data symbols are typically drawn from a fixed alphabet rather than following a Gaussian distribution. To derive an information-theoretic upper bound for throughput, we assume that each data symbol is transmitted over an AWGN channel characterized by $\mathrm{SINR}_{\ell,k}(\mathbf{H})$. We then calculate the upper limit of the throughput using the Bit Interleaved Coded Modulation (BICM) [31] capacity, denoted as

$$\begin{aligned}C_{\mathrm{BICM}} = \mathbb{E}\Bigg\{&\max_{\chi\in\{4,16,64,\ldots\}-\mathrm{QAM}}\Bigg(\log_2|\chi| \\ &-\sum_{i=1}^{\log_2|\chi|}\mathbb{E}\left\{\log_2\left\{\frac{\sum_{x\in\chi}\mathrm{PDF}(y|x)}{\sum_{x\in\chi_{\{0,1\}}^i}\mathrm{PDF}(y|x)}\right\}\right\}\Bigg)\Bigg\},\end{aligned} \tag{34}$$

where the probability density function $\mathrm{PDF}\left(y_{l,k}|x_{l,k}\right)$ is expressed as

$$\mathrm{PDF}\left(y_{l,k}|x_{l,k}\right) = \frac{1}{\pi P_{\mathrm{n}}}\exp\left(-\frac{|y_{l,k}-\tilde{h}_{l,k}x_{l,k}|^2}{P_{\mathrm{n}}}\right). \tag{35}$$

Note that instead of assuming that the data symbols are Gaussian distributed, the BICM capacity implements QAM signal constellations combined with bit interleaving. According to Eqs. (34)–(35), the upper

Table 1
Simulation parameters.

Parameter name	Value
Number of subcarriers	$L = 32$ or $L = 64$
Subcarrier spacing	$F = 15$ kHz
Carrier frequency	2.5 GHz
Number of symbols	$K_{\text{OFDM}} = 15,\ K_{\text{CP-OFDM}} = 14,\ K_{\text{FBMC}} = 30$
Sampling rate	$f_s = 10.08$ MHz
Overlapping factor	$O = 4$
Modulation order	$\{4, 16, 64\}$ – QAM

limit of system throughput can be calculated as

$$\mathcal{T}_{\text{up.}} = \frac{1}{KT}\sum_{k=1}^{K}\sum_{\ell=1}^{L/2} C_{\text{BICM,AWGN}}\left\{\text{SINR}_{\ell,k}(\mathbf{H})\right\}, \tag{36}$$

where KT denotes the duration of a subframe. Because FBMC has higher available bandwidth and requires no CP, FBMC provides a higher throughput than OFDM. However, the throughput of Pruned DCT-p-FBMC is slightly lower than conventional FBMC in high SNR. The reason is that the validity of Eq. (30) is impacted at high SNR.

5. Simulation & numerical analysis

To illustrate more clearly the potential performance of Pruned DCT-p-FBMC, we perform numerical analysis and evaluation in this section. We first evaluate the PAPR in Section 5.1. Then, in Section 5.2, we directly combine Pruned DCT-p-FBMC with MIMO and discuss the BER performance. Particularly, we also consider the 2 × 1 Alamouti's space–time block-coding technique. Finally, we discuss the throughput of SISO systems on doubly selective channels and the throughput of MIMO systems on time-varying channels. The simulation parameters are shown in Table 1.

5.1. PAPR

The FBMC signal length is much longer than T. Thus, estimating the PAPR value within one FBMC signal length is not feasible [32]. For a fair comparison with systems such as OFDM, we perform the calculation over a time spacing T (i.e., symbol period) of one symbol [33]. The detailed formula is

$$\text{PAPR} = \frac{\max\limits_{kT<t<(k+1)T}\left(|s(t)|^2\right)}{\mathbb{E}\left\{|s(t)|^2\right\}}, \quad k = 1, 2, \ldots, K. \tag{37}$$

On the other hand, for a fair comparison, we normalize the signal power (i.e., the average power of the signal is 1). Thereby, the PAPR can be simply calculated as $\max_i |[\mathbf{s}]_i|^2$. Similarly, the SNR can be simply calculated as $1/P_{\text{n}}$. The Complementary Cumulative Distribution Function (CCDF) is a commonly used metric for evaluating the performance of a signal's PAPR, which represents the probability that the signal's PAPR exceeds a certain threshold value. The detailed formula is

$$\text{CCDF}\left(10\lg(\text{PAPR})\right) = \Pr\left(\text{PAPR} > \text{PAPR}_0\right). \tag{38}$$

If we take the number of subcarriers as $L = 64$, then Fig. 6 shows the CCDF corresponding to the PAPR of the 16-QAM signal constellation. Both conventional FBMC and OFDM provide poor PAPR. Notably, Pruned DCT-p-FBMC has a slightly better PAPR than conventional FBMC. However, the PAPR of Pruned DFT-s-FBMC is slightly better than that of Pruned DCT-p-FBMC, which is benefited from the reduced time overlap between pulses [19]. Note that the aim of our scheme is to restore the biorthogonality of FBMC rather than to reduce the PAPR. However, Pruned DCT-p-FBMC obtains some advantage, although the advantage is only a 1 dB improvement.

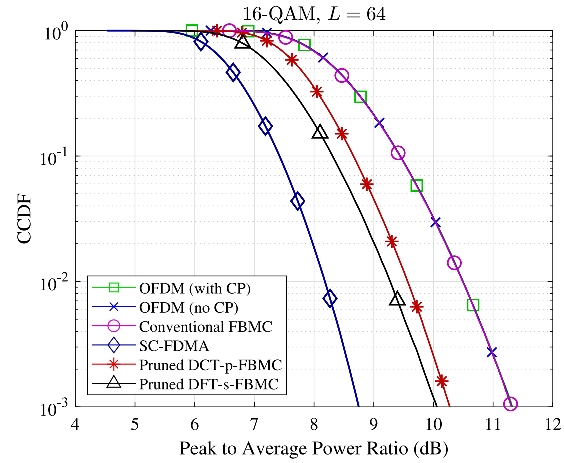

Fig. 6. Compared to OFDM, Pruned DCT-p-FBMC obtains about 1 dB improvement in PAPR and has lower OOB emission. Note that the PAPR performance of Pruned DCT-p-FBMC is about 1.5 dB worse than SC-FDMA.

5.2. BER performance

We directly combine FBMC with MIMO and then investigate the BER performance. The 2 × 2 MIMO multiplexing system model can be directly expressed as

$$\begin{bmatrix}\mathbf{r}_1\\ \mathbf{r}_2\end{bmatrix} = \begin{bmatrix}\mathbf{H}_{11} & \mathbf{H}_{12}\\ \mathbf{H}_{21} & \mathbf{H}_{22}\end{bmatrix}\begin{bmatrix}\mathbf{G}_1 & \mathbf{G}_2\end{bmatrix}\begin{bmatrix}\boldsymbol{\phi}\tilde{\mathbf{x}}_1\\ \boldsymbol{\phi}\tilde{\mathbf{x}}_2\end{bmatrix} + \begin{bmatrix}\tilde{\mathbf{n}}_1\\ \tilde{\mathbf{n}}_2\end{bmatrix}, \tag{39}$$

$$\begin{bmatrix}\mathbf{y}_1\\ \mathbf{y}_2\end{bmatrix} = \begin{bmatrix}\boldsymbol{\phi}^H\mathbf{G}_1^H & \boldsymbol{\phi}^H\mathbf{G}_2^H\end{bmatrix}\begin{bmatrix}\mathbf{r}_1\\ \mathbf{r}_2\end{bmatrix}. \tag{40}$$

Note that in achieving equalization, we need to calculate the one-tap channel with the help of $\left|\boldsymbol{\phi}^H\right|^2$. Pruned DCT-p-FBMC restores bi-orthogonality and can realize MIMO transmission in FBMC with the same complexity as in OFDM. Another advantage of Pruned DCT-p-FBMC is that all known techniques for MIMO in OFDM can be used directly.

For the 2 × 2MIMO multiplexing system of Eqs. (39)–(40), we assume that the two antennas transmit independent bit streams simultaneously. At the receiver side, we complete the detection of received symbols with ZF equalizer and ML detection. Note that the ZF equalizer ignores noise effects, and the ML detection has the disadvantage of high calculation complexity. ML technology cannot be directly applied in conventional FBMC. The reason is that imaginary interference leads to many possibilities that need to be considered for the ML technique. On the other hand, another transmission scheme we consider is 2 × 1 Alamouti's space–time block coding (which requires additional operations to be added in conventional FBMC). Defining SNR $= 10\lg\left(\frac{P_s}{P_n}\right)$dB, Fig. 7 shows the BER performance for different multicarrier schemes in a flat channel. Over a flat channel, channel-induced interference is almost zero. Thus, the validity of Eq. (30) depends only on interference and noise. When noise is dominant (i.e., SNR is below 20 dB), the equivalent of Eq. (30) is valid. Thus, the ML detection performance of Pruned DCT-p-FBMC is almost the same as that of CP-OFDM. However, the validity of Eq. (30) decreases when interference dominates (i.e., SNR is higher than 20 dB). Thus, the ML detection performance of Pruned DCT-p-FBMC appears to be different from that of CP-OFDM.

To describe the doubly selective channel, we adopt the Tap Delay Line (TDL)-A [34] power-delay profile with 120 ns delay spread in 3GPP 38.900. The mobility is set to 300 km/h. When considering frequency-selective fading, we simulate multipath transmission by increasing the number of Wide-sense Stationary Uncorrelated Scattering (WSSUS) paths. Fig. 8 shows the BER performance for different multicarrier schemes in a doubly selective channel. The conclusions in Figs. 7

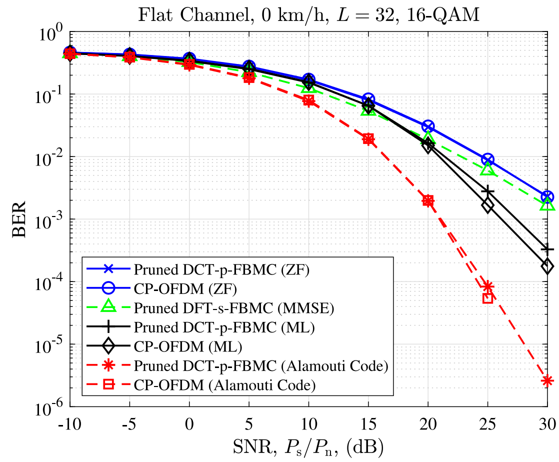

Fig. 7. BER performance of MIMO transmission and Alamouti coded transmission in a flat channel. Flat channels do not induce additional interference, so the validity of Eq. (30) depends only on the interference and noise.

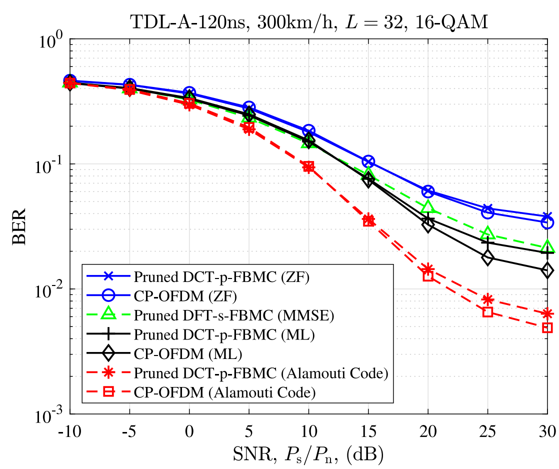

Fig. 8. BER performance of MIMO transmission and Alamouti coded transmission in a doubly selective channel. Doubly selective channels can induce additional interference. The orthogonality of Pruned DCT-p-FBMC is destroyed when interference dominates. The validity of Eq. (30) decreases, leading to a deviation in the BER performance of Pruned DCT-p-FBMC compared to OFDM.

and 8 show that many of the techniques in OFDM can be applied directly to Pruned DCT-p-FBMC (at least the diversity techniques and ML detection can be applied directly and without additional operations). It is worth noting that Pruned DFT-s-FBMC relies on truncated prototype filters. When the Pruned DFT-s-FBMC is configured with the traditional prototype filter (PHYDYAS), the interference residue is approximately 9 dB higher than that of the Pruned DCT-p-FBMC. Thus, Pruned DFT-s-FBMC performs poorly in ML and Alamouti coding techniques. We only provide its BER performance under the MMSE equalizer in Figs. 7 and 8.

5.3. Throughput

To evaluate the throughput, we adopt the modulation and coding scheme under the LTE standard. The Channel Quality Indicator (CQI) and its corresponding code rate are shown in Table 2 [35].

Note that we calculate the throughput corresponding to all constellation orders and code rates in Table 2 and select the maximum value at the receiver. This operation provides sufficient measurement for throughput ceilings without constraints on the constellation order. Since the transmitted symbols are assumed to pass through AWGN

Table 2
CQI and the corresponding code rates.

CQI Index	Modulation order	Code rate	Efficiency
1	4-QAM	78/1024	0.1523
2	4-QAM	120/1024	0.2344
3	4-QAM	193/1024	0.3770
4	4-QAM	308/1024	0.6016
5	4-QAM	449/1024	0.8770
6	4-QAM	602/1024	1.1758
7	16-QAM	378/1024	1.4766
8	16-QAM	490/1024	1.9141
9	16-QAM	616/1024	2.4063
10	64-QAM	466/1024	2.7305
11	64-QAM	567/1024	3.3223
12	64-QAM	666/1024	3.9023
13	64-QAM	772/1024	4.5234
14	64-QAM	873/1024	5.1152
15	64-QAM	948/1024	5.5547

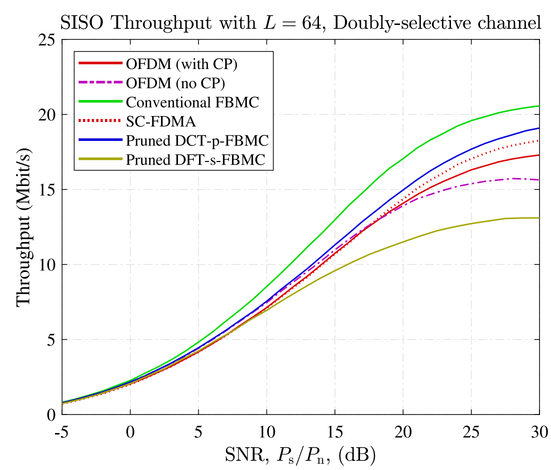

Fig. 9. Throughput for SISO transmissions in doubly selected channels. Pruned DCT-p-FBMC is superior to OFDM due to more robustness to time-varying channels and requires no CP.

channels characterized by both noise and interference (i.e., SINR ($\mathbf{H}$)), we calculate the LLR required for Turbo decoding under AWGN channel conditions. Thus, the throughput calculation relies only on $|\tilde{h}_{\ell,k}|^2/P_n$. If there are infinitely many transmitted blocks in time, then the throughput can be calculated as $\mathbb{E}_{\mathbf{H}}\{\mathcal{T}_{\text{up.}}\}$, see Eq. (36). However, in practice, L and K are finite. Thus, in the subsequent simulations, we adopt $\mathbb{E}_{|\tilde{h}_{\ell,k}|}\left\{\mathcal{T}_{\text{up.}}(|\tilde{h}_{\ell,k}|^2/P_n)\right\}$ to calculate the throughput.

Considering higher delay spread, we set the channel parameter to TLD-A-300ns and set the mobility to 200 km/h. For the SISO system in a doubly selective channel, Fig. 9 shows the throughput for different multicarrier modulation systems. We can observe that the throughput of Pruned DCT-p-FBMC is about 5% better than SC-FDMA. Additionally, our scheme requires no CP, which further improves throughput. The throughput of Pruned DFT-s-FBMC with conventional prototype filter is lowest at high SNR. The reason is that the power of the residual interference is higher than noise and the calculation of the LLR does not consider the interference.

On the other hand, conventional FBMC has higher throughput than our scheme. The reason is that precoding leads to an averaging effect in the channel. Note that for throughput values with SNR below 17.5 dB, OFDM without CP outperforms OFDM with CP. However, at SNR higher than 17.5 dB, the throughput of OFDM without CP decreases. The reason for this mismatch is that we employ the very simple LLR calculation method, see Eq. (31). The calculation implicitly ignores channel-induced interference.

Considering low delay spreading, we set the channel parameter to TLD-A-10ns and set the mobility to 400 km/h. For MIMO systems

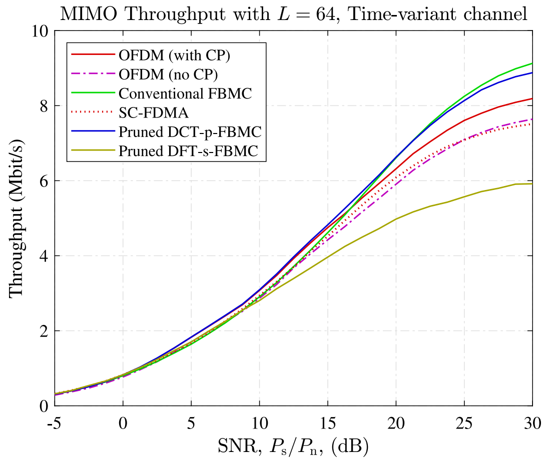

Fig. 10. Throughput of MIMO transmission in time-varying channels. If the delay spread is low enough, the throughput of Pruned DCT-p-FBMC will be closer to that of conventional FBMC.

in time-varying channels, Fig. 10 shows the throughput for different multicarrier systems. We can observe that the throughput of Pruned DCT-p-FBMC is approximately the same as that of conventional FBMC. However, at the SNR of 23 dB, the throughput of Pruned DCT-p-FBMC shows a deviation of 0.5% from that of conventional FBMC. The reason is that interference is beginning to dominate. Similarly, the throughput of Pruned DFT-s-FBMC with conventional prototype filter is lowest at high SNR due to residual interference.

6. Conclusion

In this paper, we propose the Pruned DCT Precoding based FBMC Modulation scheme. The scheme outperforms OFDM in many aspects, e.g., Pruned DCT-p-FBMC is more robust to doubly selective channels, low OOB emission, etc. In particular, Pruned DCT-p-FBMC can approximately equate to OFDM orthogonal transmission, achieving compatibility with OFDM. Therefore, Pruned DCT-p-FBMC can directly apply many known techniques in OFDM, e.g., ML detection techniques, Turbo coding, etc. Once we employ Pruned DCT precoding, FBMC can be directly combined with MIMO technology without additional calculation. The good time–frequency properties of Pruned DCT-p-FBMC ensure that no strict synchronization authorization is required between multiple users. However, the underlying system of Pruned DCT-p-FBMC is still OQAM-FBMC, and thus, its complexity is not reduced compared to conventional FBMC.

CRediT authorship contribution statement

Ying Wang: Writing – original draft, Validation, Supervision, Software, Methodology, Conceptualization. **Qiang Guo:** Writing – review & editing. **Jianhong Xiang:** Project administration, Data curation. **Yu Zhong:** Funding acquisition.

Declaration of competing interest

The authors declare that they have no known competing financial interests or personal relationships that could have appeared to influence the work reported in this paper.

Acknowledgments

This work is supported in part by Fundamental Research Funds for the Central Universities, China [3072022CF0801], and Sichuan Provincial Key Laboratory of Agile Intelligent Computing Project.

Appendix A. Detailed derivation of Eqs. (10)–(11).

For simplicity of representation, we express Eq. (8) in discrete time form, that is

$$g_{l,k}(n) = \left[\mathbf{g}_{l,k}\right]_n. \tag{41}$$

Then, the discrete-time form $s(n)$ of the transmitted signal $s(t)$ can be expressed as

$$s(n) = \sum_{l=1}^{L}\sum_{k=1}^{K} x_{l,k} g_{l,k}(n). \tag{42}$$

If the sample values of all the transmitted signals are stacked in the vector $\mathbf{s} \in \mathbb{C}^{N\times 1}$, then Eq. (42) can be expressed in matrix form as

$$\mathbf{s} = \left[\mathbf{g}_{1,1}, \ldots, \mathbf{g}_{L,K}\right]\begin{bmatrix} x_{1,1} \\ \vdots \\ x_{L,K}\end{bmatrix} = \mathbf{Gx}. \tag{43}$$

Assuming that the channel "TDL-A" has P transmission paths, we can express the discrete time-varying impulse response $h\left(n, \tau_p\right)$ by a banded convolution matrix $\mathbf{H} \in \mathbb{C}^{N\times N}$ [6], that is

$$[\mathbf{H}]_{i,j} = h(i, i-j). \tag{44}$$

Then, the discrete-time model of Eq. (2) can be expressed as

$$r(n) = \sum_{p=1}^{P} h\left(n, \tau_p\right) s\left(n-\tau_p\right) + \bar{\mathrm{n}}(n). \tag{45}$$

If the sample values of all received signals are stacked in the vector $\mathbf{r} \in \mathbb{C}^{N\times 1}$, Eq. (45) can be expressed as

$$\mathbf{r} = \mathbf{Hs} + \bar{\mathbf{n}} = \mathbf{HGx} + \bar{\mathbf{n}}. \tag{46}$$

For the received symbol $y_{l,k}$, we can express Eq. (3) in discrete-time form as

$$y_{l,k} = \sum_{n=1}^{N} r(n)\, g_{l,k}^{*}(n). \tag{47}$$

Eq. (47) can be expressed in matrix form as

$$y_{l,k} = \mathbf{g}_{l,k}^{*}\mathbf{r}. \tag{48}$$

If all the received symbols are stacked in the vector $\mathbf{y} \in \mathbb{C}^{LK\times 1}$, then $\mathbf{y} \in \mathbb{C}^{LK\times 1}$ can be expressed in matrix form as

$$\mathbf{y} = \mathbf{G}^H\mathbf{r} = \mathbf{G}^H\mathbf{HGx} + \mathbf{n}. \tag{49}$$

If the Doppler spread and Delay spread of the channel are low enough, then $\mathbf{H}$ can be approximated as a diagonal matrix. At this time, according to Eqs. (6) and (44), the (l,k)th received symbol $y_{l,k}$ can be expressed as

$$\begin{aligned} &y_{l,k} \\ &= \left(\sum_{n=1}^{N} h(n,0)\, g_{l,k}(n)\, g_{l,k}^{*}(n)\right)\left(x_{l,k} + \mathrm{j}\Im\{\mathbf{q}_{l,k}\}\mathbf{x}\right) + \mathrm{n}_{l,k}, \\ &= \mathbf{g}_{l,k}^{H}\mathbf{HGx} + \mathbf{n}_{l,k} \end{aligned} \tag{50}$$

where $\mathbf{q}_{l,k} = [\mathbf{G}^H\mathbf{G}]_{l+kL}$. If the channel-induced interference can be ignored, then the FBMC has only inherent imaginary interference, that is

$$\begin{aligned} y_{l,k} &= \mathbf{g}_{l,k}^{H}\mathbf{HGx} + \mathbf{n}_{l,k} \\ &= H_{l,k}\mathbf{g}_{l,k}^{H}\mathbf{Gx} + \mathbf{n}_{l,k} \end{aligned}. \tag{51}$$

To obtain the matrix representation of $H_{l,k}$, we express the convolution sum in Eq. (50) as

$$\begin{aligned} H_{l,k} &= \sum_{n=1}^{N}\left[\left(\mathbf{g}_{l,k}^{H}\mathbf{H}\right)\circ\mathbf{g}_{l,k}^{T}\right]_n \\ &= \left[\mathrm{diag}\left\{\mathbf{G}^H\mathbf{HG}\right\}\right]_{l+kL} \end{aligned}. \tag{52}$$

Considering all received symbols, Eq. (51) can be expressed as

$$\mathbf{y} = \mathrm{diag}\left\{\mathbf{G}^H\mathbf{HG}\right\}\mathbf{G}^H\mathbf{Gx} + \mathbf{n}. \tag{53}$$

Appendix B. Detailed derivation of Eq. (33)

If channel gain is considered, we need to apply the generalized LLR expression, that is

$$LLR\left(b_i\right) = \log \frac{\sum_{\tilde{x}_{\ell,k}\in\chi_1^i} \mathrm{PDF}\left(\tilde{y}_{\ell,k}\left|\tilde{x}_{\ell,k}\right.,\tilde{h}_{\ell,k}\right)}{\sum_{\tilde{x}_{\ell,k}\in\chi_0^i} \mathrm{PDF}\left(\tilde{y}_{\ell,k}\left|\tilde{x}_{\ell,k}\right.,\tilde{h}_{\ell,k}\right)}. \tag{54}$$

where

$$\begin{aligned}
&\mathrm{PDF}\left(\tilde{y}_{\ell,k}\left|\tilde{x}_{\ell,k}\right.,\tilde{h}_{\ell,k}\right)\\
&= \frac{1}{\pi P_{\mathrm{n}}^{\ell,k}} \exp\left\{\frac{-\left|\tilde{y}_{\ell,k}-\tilde{h}_{\ell,k}\tilde{x}_{\ell,k}\right|^2}{P_{\mathrm{n}}^{\ell,k}}\right\}\\
&= \frac{1}{\pi P_{\mathrm{n}}^{\ell,k}} \exp\left\{-\left|\sqrt{\left(P_{\mathrm{n}}^{\ell,k}\right)^{-1}}\left(\tilde{y}_{\ell,k}-\tilde{h}_{\ell,k}\tilde{x}_{\ell,k}\right)\right|^2\right\}
\end{aligned}. \tag{55}$$

According to Eq. (30), we need to calculate the noise power corresponding to each symbol. The noise correlation matrix (i.e., the covariance matrix of $\tilde{\mathbf{n}}$) can be calculated as

$$\begin{aligned}
\mathbf{R}_{\mathrm{n}} &= \mathbb{E}\left\{\tilde{\mathbf{n}}\tilde{\mathbf{n}}^H\right\}\\
&= \sqrt{P_{\mathrm{n}}}\tilde{\mathbf{G}}^H\left(\sqrt{P_{\mathrm{n}}}\tilde{\mathbf{G}}^H\right)^H\\
&= P_{\mathrm{n}}\tilde{\mathbf{G}}^H\tilde{\mathbf{G}}
\end{aligned}. \tag{56}$$

It is worth noting that $\tilde{\mathbf{G}}^H\tilde{\mathbf{G}} \approx \mathbf{I}_{LK/2}$ leads to differences in the noise power corresponding to each symbol. Therefore, substituting P_n directly into Eq. (55) is not entirely accurate. Alternatively, we directly perform a singular value decomposition for $\mathbf{R}_{\mathrm{n}}^{-1}$ and directly calculate the $\sqrt{\left(P_{\mathrm{n}}^{\ell,k}\right)^{-1}}$ required by Eq. (55). That is

$$\begin{aligned}
&\mathcal{G}_{\mathrm{n}}^{\ell,k} = \sqrt{\left(P_{\mathrm{n}}^{\ell,k}\right)^{-1}} = \mathrm{diag}\left(\mathbf{S}\sqrt{\mathbf{V}}\mathbf{U}^H\right)_{\ell+L(k-1)/2}\\
&st.\ \mathbf{R}_{\mathrm{n}}^{-1} = \mathbf{S}\mathbf{V}\mathbf{U}^H
\end{aligned}. \tag{57}$$

where $\mathbf{S} \in \mathbb{C}^{LK/2\times LK/2}$ denotes the left singular vector matrix, $\mathbf{V} \in \mathbb{C}^{LK/2\times LK/2}$ denotes the singular value matrix, and $\mathbf{U} \in \mathbb{C}^{LK/2\times LK/2}$ denotes the right singular vector matrix.

Data availability

Available Code can be downloaded at https://github.com/WangYeeng/Pruned-DCT-P-FBMC_master.

References

[1] Gerhard Wunder, Peter Jung, Martin Kasparick, Thorsten Wild, Frank Schaich, Yejian Chen, Stephan Ten Brink, Ivan Gaspar, Nicola Michailow, Andreas Festag, et al., 5GNOW: Non-orthogonal, asynchronous waveforms for future mobile applications, IEEE Commun. Mag. 52 (2) (2014) 97–105.

[2] Behrouz Farhang-Boroujeny, OFDM versus filter bank multicarrier, IEEE Signal Process. Mag. 28 (3) (2011) 92–112.

[3] Behrouz Farhang-Boroujeny, Hussein Moradi, OFDM inspired waveforms for 5G, IEEE Commun. Surv. Tutor. 18 (4) (2016) 2474–2492.

[4] Ying Wang, Qiang Guo, Jianhong Xiang, Linyu Wang, Yang Liu, Bi-orthogonality recovery and MIMO transmission for FBMC Systems based on non-sinusoidal orthogonal transformation, Signal Process. (2024) 109427.

[5] Iandra Galdino Andrade, Didier Le Ruyet, Marcello LR de Campos, Rostom Zakaria, Bit error probability expressions for QAM-FBMC systems, IEEE Commun. Lett. 26 (5) (2022) 994–998.

[6] Ronald Nissel, Stefan Schwarz, Markus Rupp, Filter bank multicarrier modulation schemes for future mobile communications, IEEE J. Sel. Areas Commun. 35 (8) (2017) 1768–1782.

[7] Mario Tanda, Asymptotic performance of FBMC-PAM systems in frequency-selective Rayleigh fading channels, Signal Process. 201 (2022) 108693.

[8] Yuhao Qi, Jian Dang, Zaichen Zhang, Liang Wu, Yongpeng Wu, Efficient channel equalization and performance analysis for uplink FBMC/OQAM-Based massive MIMO systems, IEEE Trans. Veh. Technol. 72 (9) (2023) 11532–11547.

[9] Hans G. Feichtinger, Thomas Strohmer, Gabor Analysis and Algorithms: Theory and Applications, Springer Science & Business Media, 2012.

[10] Alphan Sahin, Ismail Guvenc, Huseyin Arslan, A survey on multicarrier communications: Prototype filters, lattice structures, and implementation aspects, IEEE Commun. Surv. Tutor. 16 (3) (2013) 1312–1338.

[11] Ying Wang, Qiang Guo, Jianhong Xiang, Yang Liu, Doubly selective channel estimation and equalization based on ICI/ISI mitigation for OQAM-FBMC systems, Phys. Commun. 59 (2023) 102120.

[12] Rostom Zakaria, Didier Le Ruyet, A novel filter-bank multicarrier scheme to mitigate the intrinsic interference: Application to MIMO systems, IEEE Trans. Wireless Commun. 11 (3) (2012) 1112–1123.

[13] Miquel Payaró, Antonio Pascual-Iserte, Montse Nájar, Performance comparison between FBMC and OFDM in MIMO systems under channel uncertainty, in: 2010 European Wireless Conference, EW, IEEE, 2010, pp. 1023–1030.

[14] Pascal Chevalier, Didier Le Ruyet, Remi Chauvat, Maximum likelihood alamouti receiver for filter bank based multicarrier transmissions, in: WSA 2016; 20th International ITG Workshop on Smart Antennas, VDE, 2016, pp. 1–7.

[15] Han Wang, Lingwei Xu, Zhengqiang Yan, T. Aaron Gulliver, Low-complexity MIMO-FBMC sparse channel parameter estimation for industrial big data communications, IEEE Trans. Ind. Inform. 17 (5) (2020) 3422–3430.

[16] Rostom Zakaria, Didier Le Ruyet, Theoretical analysis of the power spectral density for FFT-FBMC signals, IEEE Commun. Lett. 20 (9) (2016) 1748–1751.

[17] Ronald Nissel, Jiri Blumenstein, Markus Rupp, Block frequency spreading: A method for low-complexity MIMO in FBMC-OQAM, in: 2017 IEEE 18th International Workshop on Signal Processing Advances in Wireless Communications, SPAWC, IEEE, 2017, pp. 1–5.

[18] Ronald Nissel, Markus Rupp, Enabling low-complexity MIMO in FBMC-OQAM, in: 2016 IEEE Globecom Workshops, GC Wkshps, IEEE, 2016, pp. 1–6.

[19] Ronald Nissel, Markus Rupp, Pruned DFT-spread FBMC: Low PAPR, low latency, high spectral efficiency, IEEE Trans. Commun. 66 (10) (2018) 4811–4825.

[20] Stefania Sesia, Issam Toufik, Matthew Baker, LTE-the UMTS Long Term Evolution: from Theory to Practice, John Wiley & Sons, 2011.

[21] Markku Renfors, Tero Ihalainen, Tobias Hidalgo Stitz, A block-Alamouti scheme for filter bank based multicarrier transmission, in: 2010 European Wireless Conference, EW, IEEE, 2010, pp. 1031–1037.

[22] Dongjun Na, Kwonhue Choi, Intrinsic ICI-free Alamouti coded FBMC, IEEE Commun. Lett. 20 (10) (2016) 1971–1974.

[23] Qiang Guo, Ying Wang, Jianhong Xiang, Yu Zhong, Complex Gaussian ratio-based bit error probability calculation for PAM-FBMC systems, IEEE Commun. Lett. 28 (4) (2024) 788–792.

[24] Hosseinali Jamal, David W. Matolak, Dual-polarization FBMC for improved performance in wireless communication systems, IEEE Trans. Veh. Technol. 68 (1) (2018) 349–358.

[25] Pierre Siohan, Cyrille Siclet, Nicolas Lacaille, Analysis and design of OFDM/OQAM systems based on filterbank theory, IEEE Trans. Signal Process. 50 (5) (2002) 1170–1183.

[26] Maurice Bellanger, D. Le Ruyet, D. Roviras, M. Terré, J Nossek, L Baltar, Q Bai, D Waldhauser, M Renfors, T Ihalainen, et al., FBMC physical layer: a primer, in: PHYDYAS, January, vol. 25, 2010, pp. 7–10.

[27] Georg Taubock, Franz Hlawatsch, A compressed sensing technique for OFDM channel estimation in mobile environments: Exploiting channel sparsity for reducing pilots, in: 2008 IEEE International Conference on Acoustics, Speech and Signal Processing, IEEE, 2008, pp. 2885–2888.

[28] Alan V. Oppenheim, Ronald W. Schafer, John R. Buck, Discrete-Time Signal Processing, Prentice-Hall, Inc, 1999.

[29] Ralf Haas, Jean-Claude Belfiore, A time-frequency well-localized pulse for multiple carrier transmission, Wirel. Pers. Commun. 5 (1997) 1–18.

[30] B. Le Flch, M. Alard, C. Berrou, Coded orthogonal frequency-division multiplexing, Proc. IEEE 83 (6) (1995) 982–996.

[31] Giuseppe Caire, Giorgio Taricco, Ezio Biglieri, Bit-interleaved coded modulation, IEEE Trans. Inform. Theory 44 (3) (1998) 927–946.

[32] Ji-Hyun Moon, Ye-Ri Nam, Jeong-Ho Kim, PAPR reduction in the FBMC-OQAM system via segment-based optimization, IEEE Access 6 (2018) 4994–5002.

[33] Dongjun Na, Kwonhue Choi, Low papr fbmc, IEEE Trans. Wireless Commun. 17 (1) (2017) 182–193.

[34] Study on channel model for frequency spectrum above 6 GHz; (Release 14), 2016, 3GPP, TR 38.900.

[35] T. ETSI, 136 213 V8. 8.0 (2009–10), 2010, pp. 136200–136299, Technical Specification– LTE.